



CONDENSED MATTER PHYSICS

Superconductivity due to fluctuating loop currents

Grgur Palle^{1*}, Risto Ojajarvi¹, Rafael M. Fernandes², Jörg Schmalian^{1,3}

Orbital magnetism and the loop currents (LCs) that accompany it have been proposed to emerge in many systems, including cuprates, iridates, and kagome superconductors. In the case of cuprates, LCs have been put forward as the driving force behind the pseudogap, strange-metal behavior, and $d_{x^2-y^2}$ -wave superconductivity. Here, we investigate whether fluctuating intra-unit-cell LCs can cause unconventional superconductivity. For odd-parity LCs, we find that they are repulsive in all pairing channels near the underlying quantum-critical point (QCP). For even-parity LCs, their fluctuations give rise to unconventional pairing, which is not amplified in the vicinity of the QCP, in sharp contrast to pairing mediated by spin-magnetic, nematic, or ferroelectric fluctuations. Applying our formalism to the cuprates, we conclude that fluctuating intra-unit-cell LCs are unlikely to yield $d_{x^2-y^2}$ -wave superconductivity. If LCs are to be relevant for the cuprates, they must break translation symmetry.

INTRODUCTION

Although magnetic order most commonly arises from interactions related to the spin degrees of freedom, in correlated systems magnetism may also develop in the orbital sector. Whenever such orbital magnetism occurs, time-reversal symmetry breaking manifests itself through a pattern of spontaneously flowing currents. This pattern must be made of closed loops to avoid a global current, forbidden due to a theorem by Bloch (1–3). Through the years, many types of loop-current (LC) patterns have been proposed in a variety of systems.

In the cuprates, inversion symmetry-breaking intra-unit-cell LCs have been put forward as the underlying order of the pseudogap state (4–6), while their fluctuations have been proposed to drive both $d_{x^2-y^2}$ -wave superconductivity (7) and marginal Fermi liquid behavior near the quantum-critical point (QCP) (8, 9). Cuprate LC order was also invoked to explain polarized neutron scattering experiments (10–14). However, in another experiment, performed using polarized neutrons, no evidence for LC order could be detected (15). Nuclear magnetic resonance (NMR) measurements also failed to observe LC order (16, 17) of a magnitude comparable to that predicted theoretically (18). Furthermore, recent muon spin relaxation measurements (19, 20) found no evidence for LC order in the pseudogap state and were used to argue that the effects of LCs on NMR relaxation rates are too small to be observable (20).

Apart from cuprates, a state consistent with LC order has been inferred from second-harmonic generation measurements in the iridate Mott insulator Sr_2IrO_4 (21), which displays an unusual gap upon doping (22, 23). An LC pattern that breaks translation symmetry is one of the main candidates for explaining why the charge-density wave displayed by the recently discovered kagome superconductors seemingly breaks time-reversal symmetry (24). Beyond specific materials, LCs have also been discussed in the context of the spontaneous anomalous Hall effect in Fermi liquids (25–27) and in the context of spin liquids with broken time-reversal symmetry (28).

Given their potential realization in a diverse set of systems, it is important to elucidate whether fluctuating LCs can give rise to

superconductivity. In this context, intra-unit-cell (i.e., $\mathbf{q} = 0$) LCs have been prominently discussed as the pairing glue of the cuprates, which makes them especially interesting, notwithstanding the difficulties in detecting them. For comparison, in the case of fluctuations from intra-unit-cell orders that preserve time-reversal symmetry, such as nematic (29–31) and ferroelectric (32, 33) ones, it is well established that s-wave pairing generally emerges with a number of attractive subleading channels. Moreover, superconductivity in these cases is strongly enhanced as the QCP is approached, thus establishing a robust regime in which pairing is dominated by the corresponding fluctuations. Pairing is promoted by ferromagnetic spin fluctuations (34, 35) as well, the main difference being the p-wave nature of the leading pairing state. However, the case of pure orbital magnetism is different, not only because LCs do not directly couple to the spin but also because they usually break additional symmetries besides time reversal. This leads to two important questions of broad and particular relevance. First, are there general conditions, independent of the details of a given material, under which pairing is dominated by quantum-critical intra-unit-cell LC fluctuations? Second, in the specific case of the cuprates, can fluctuating intra-unit-cell LCs cause or enhance $d_{x^2-y^2}$ -wave pairing?

Here, we answer both questions. We show that LC fluctuations do not give rise to an enhanced pairing near the QCP, as shown schematically in Fig. 1. Even-parity LCs, such as orbital ferromagnets or orbital altermagnets, may cause unconventional pairing. However, they are as likely or unlikely to do so as any other degree of freedom far from its critical point. This is because the pairing promoted by these fluctuations is not enhanced as the QCP is approached (orange line in Fig. 1), in sharp contrast to the cases of ferromagnetic spin fluctuations or time-reversal-even charge fluctuations, such as nematic or ferroelectric ones (blue line in Fig. 1). LCs that break parity, i.e., states of magneto-electric order, are repulsive for all pairing symmetries as one approaches the QCP (green line in Fig. 1). Hence, they weaken pairing caused by other mechanisms. Such odd-parity LC states can at best support superconductivity when their fluctuations are sufficiently weak. In the context of the cuprates, we show that among the three candidate LC states, shown in Fig. 2 (B to D), only the fluctuations of the parity-preserving d-wave LC favor weak $d_{x^2-y^2}$ -wave pairing (Figs. 3 and 4). In the presence of weak spin-orbit coupling, triplet pairing mediated by secondary spin-magnetic fluctuations takes place (Fig. 5) and always prevails for d-wave LCs as the QCP is approached.

¹Institute for Theoretical Condensed Matter Physics, Karlsruhe Institute of Technology, 76131 Karlsruhe, Germany. ²School of Physics and Astronomy, University of Minnesota, Minneapolis, MN 55455, USA. ³Institute for Quantum Materials and Technologies, Karlsruhe Institute of Technology, 76131 Karlsruhe, Germany. *Corresponding author. Email: grgur.palle@kit.edu

Copyright © 2024 the Authors, some rights reserved; exclusive licensee American Association for the Advancement of Science. No claim to original U.S. Government Works. Distributed under a Creative Commons Attribution License 4.0 (CC BY).

Downloaded from https://www.science.org at KIT Library on June 19, 2024

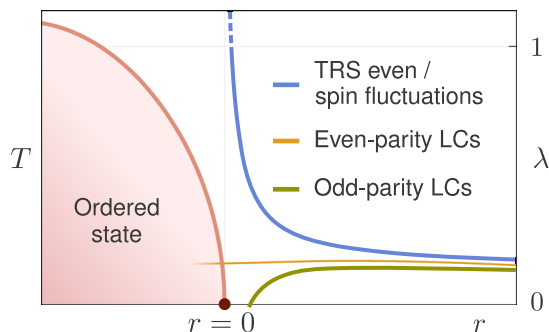


Fig. 1. Schematic behavior of the leading pairing eigenvalue λ as a QCP is approached from the disordered side. The QCP is controlled by the tuning parameter r . The superconducting transition temperature grows with λ according to $T_c \propto \omega_c e^{-1/\lambda}$. Pairing mediated by time-reversal-even charge fluctuations or spin fluctuations (blue) is enhanced near the QCP, where weak-coupling theory breaks down (dashed line). In contrast, we find that the pairing mediated by even-parity LCs (orange) is not enhanced at the QCP, whereas pairing mediated by odd-parity LCs (green) becomes strongly repulsive near the QCP.

We treat the interactions phenomenologically and assume from the outset that they give rise to intra-unit-cell orbital magnetism and LCs.

Under these assumptions, the interacting Hamiltonian $H_{\text{int}} = g \sum_{\mathbf{q}} \Phi_{-\mathbf{q}} \phi_{\mathbf{q}}$ can be described in terms of a coupling between the fluctuating LC order parameter $\Phi_{\mathbf{q}}$ and a symmetry-appropriate fermionic bilinear

$$\phi_{\mathbf{q}} = \frac{1}{\sqrt{N}} \sum_{\mathbf{k}} c_{\mathbf{k}}^{\dagger} \Gamma_{\mathbf{k}, \mathbf{k}+\mathbf{q}} c_{\mathbf{k}+\mathbf{q}} \quad (1)$$

Here, N is the number of unit cells and g is the coupling constant. The orbital LC pattern associated with $\Phi_{\mathbf{q}}$ is encoded in the form factor $\Gamma_{\mathbf{k}, \mathbf{p}} = \Gamma_{\mathbf{p}, \mathbf{k}}^{\dagger}$, which is a matrix in spin and orbital space. In the absence of spin-orbit coupling, these form factors are trivial in spin space, meaning $\Gamma_{\mathbf{k}, \mathbf{p}} = \gamma_{\mathbf{k}, \mathbf{p}} \otimes \sigma^0$, where σ^0 is the identity matrix in spin space. Consequently, the orbital matrix must be odd under time reversal, $\gamma_{\mathbf{k}, \mathbf{p}}^* = -\gamma_{-\mathbf{k}, -\mathbf{p}}$.

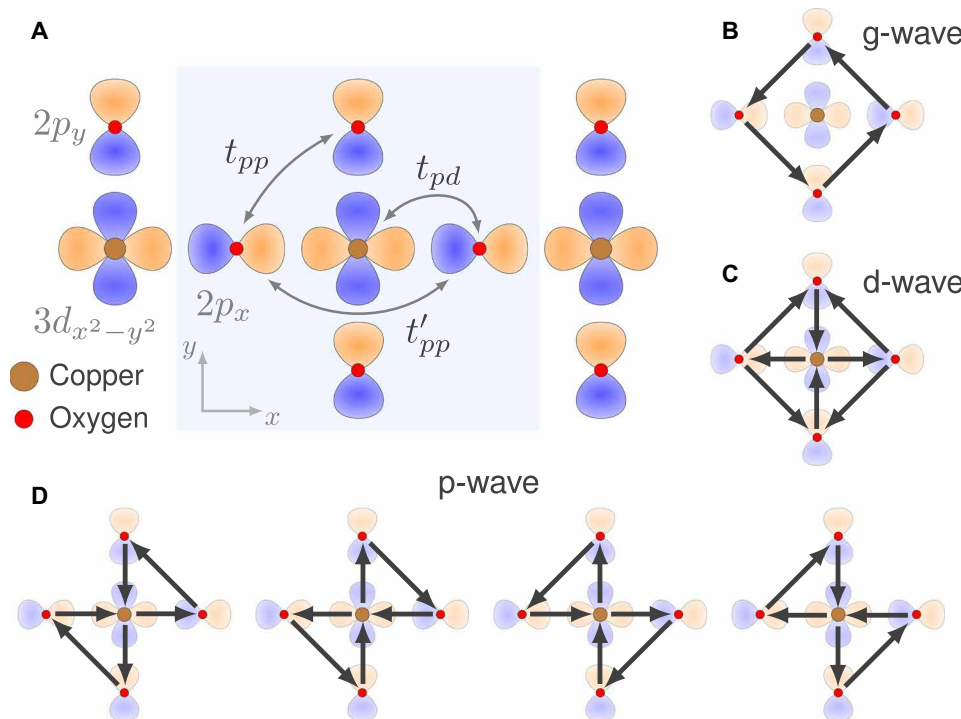


Fig. 2. Orbitals and LC patterns of the CuO_2 planes of cuprates. (A) CuO_2 plane and its active orbitals. Arrows denote hoppings included in our model. Light blue shading highlights the five orbitals used to form LCs. (B to D) Three possible LC patterns of the CuO_2 plane with (B) $g_{xy(x^2-y^2)}$, (C) $d_{x^2-y^2}$, and (D) (p_x, p_y) character. While the last one has the symmetry of a four-state clock model, as indicated by the four degenerate patterns, the former two display Ising symmetry.

RESULTS

Formalism

We start with a general analysis that allows us to draw conclusions that are independent of material details. Consider a centrosymmetric system with M orbitals per primitive unit cell and introduce the spinors $c_{\mathbf{k}\sigma} = (c_{\mathbf{k}\sigma 1}, \dots, c_{\mathbf{k}\sigma M})^T$ and $c_{\mathbf{k}} = (c_{\mathbf{k}\uparrow}, c_{\mathbf{k}\downarrow})^T$ in terms of which the one-particle Hamiltonian equals $H_0 = \sum_{\mathbf{k}} c_{\mathbf{k}}^{\dagger} H_{\mathbf{k}} c_{\mathbf{k}}$. For H_0 , we assume that it preserves parity and time-reversal symmetry.

LC fluctuations are described by the $\Phi_{\mathbf{q}}$ correlation function $\chi(\mathbf{q}, \omega)$, which we assume to be peaked at $\mathbf{q} = 0$ in momentum space and characterized by a correlation length $\xi = a_0 r^{-\nu}$, where a_0 is a microscopic length scale. r is a dimensionless parameter that, by definition, vanishes at the QCP and is $r \sim 1$ for a structureless correlation function in momentum space. For the static correlation function,

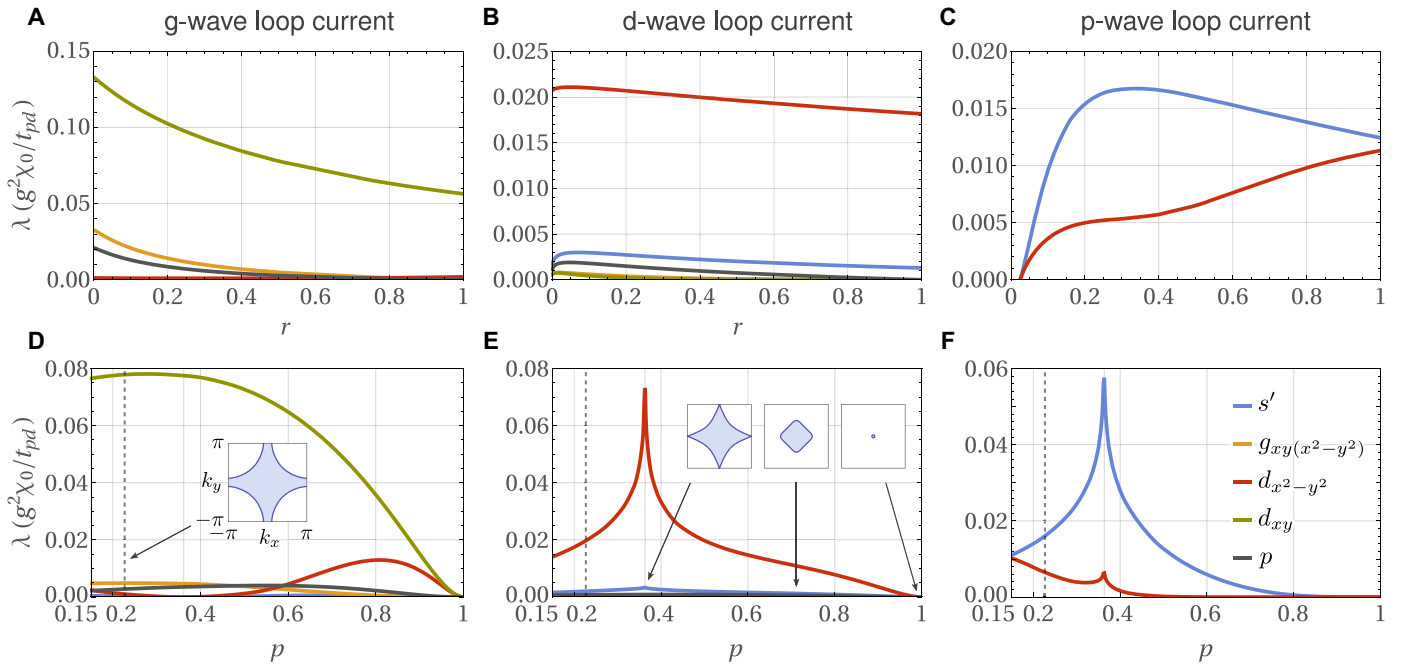


Fig. 3. Strength of the pairing tendency due to LC fluctuations, as a function of distance from QCP and chemical potential. (A to C) Pairing eigenvalues λ (Eq. 2) for the three LC states of Fig. 2 as a function of the parameter r characterizing the proximity to the QCP at fixed chemical potential $\mu = 0.9t_{pd}$. (D to F) Eigenvalues at fixed $r = 0.5$ as a function of the hole doping p . The dashed vertical lines in (D) to (F) denote the hole doping $p = 0.23$ corresponding to $\mu = 0.9t_{pd}$. The insets in (D) and (E) illustrate the Fermi surfaces at different values of p . The Lifshitz transition occurs at $p = 0.36$. Φ_g [(A) and (D)] and Φ_d [(B) and (E)] fluctuations yield d_{xy} and $d_{x^2-y^2}$ pairing, respectively, that is only weakly enhanced near the QCP. Φ_p fluctuations (C) yield extended s -wave pairing (denoted s') at not too small r , turning repulsive as the QCP is approached ($r \rightarrow 0$). There is a one-parameter family of possible Φ_p parameterized by α (Fig. 4). In (C) and (F), we use $\alpha = 0$.

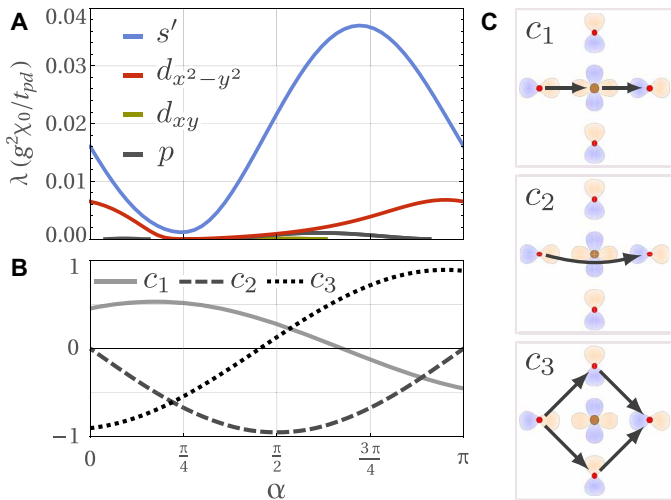


Fig. 4. The pairing tendency and the composition of the one-parameter family of possible p-wave LC orders. (A) Pairing eigenvalues λ (Eq. 2) due to p-wave LC fluctuations as a function of α for fixed $r = 0.5$ and $\mu = 0.90t_{pd}$. s' refers to an extended s -wave state dominated by $\cos(4\varphi)$ dependence on the Fermi surface angle φ . (B) α parametrizes the coefficients of the three p-wave current components $c_{1,2,3}$ illustrated in (C). The coefficients $c_{1,2,3}$ are constrained to not generate a global current (Methods D).

we use the critical scaling expression $\chi(\mathbf{q}) = F(q\xi)/q^{2-\eta}$ with critical exponents ν and η , and scaling function $F(y)$ that has the usual asymptotic behaviors $F(y \gg 1) \sim \text{const.}$ and $F(y \ll 1) \sim y^{2-\eta}$.

Solving this coupled many-body problem is a formidable challenge. To make progress, we follow the strategy of (7, 29) and consider the system in the regime where the coupling of the electrons to LC fluctuations is sufficiently weak ($g \rightarrow 0$). This allows us to analyze the pairing instability to leading order in perturbation theory. Such a strategy should be reasonable on the disordered side, far enough from the QCP, where Fermi liquid behavior is established and collective fluctuations are sufficiently weak. This approach enables us to determine whether or not the weak-coupling theory breaks down as one approaches the QCP, thus providing an indicator for strong quantum-critical pairing.

In the weak-coupling limit, it is straightforward to derive the linearized gap equation for the singlet and triplet pairing channels (Methods A):

$$\int_{\text{FS}} \frac{dS_{\mathbf{k}}}{(2\pi)^d v_{\mathbf{k}}} V_s(\mathbf{p}, \mathbf{k}) \Delta_s(\mathbf{k}) = \lambda \Delta_s(\mathbf{p}) \quad (2)$$

Here, the integral goes over the Fermi surface, $v_{\mathbf{k}} = |\nabla \epsilon_{\mathbf{k}}|$ is the Fermi velocity, and $s = +1$ (-1) stands for singlet (triplet) pairing. The largest positive eigenvalue λ determines the superconducting transition temperature through $k_B T_c = (2e^2/\pi)\omega_c e^{-1/\lambda}$, where ω_c is the characteristic cutoff for LC fluctuations and γ is the Euler-Mascheroni constant. The eigenvector $\Delta_s(\mathbf{p})$ determines the symmetry of the pairing and is related to the superconducting

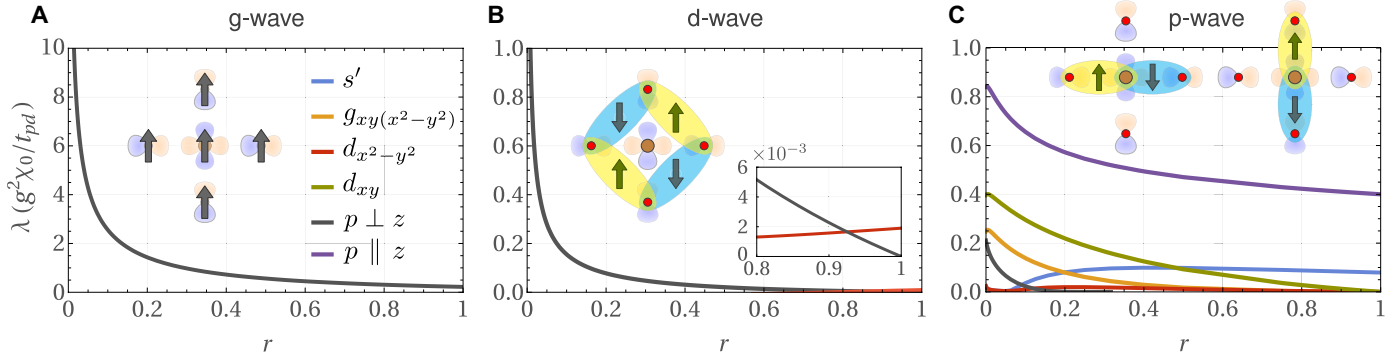


Fig. 5. Strength of the pairing tendency due to spin fluctuations that are symmetry-equivalent to LCs, as a function of distance from QCP. The panels show the pairing eigenvalues λ (Eq. 2) due to spin fluctuations as a function of r at fixed $\mu = 0.90t_{pd}$. In the presence of spin-orbit coupling, these secondary spin fluctuations are triggered by the orbital LC order parameters Φ_g (A), Φ_d (B), and Φ_p (C). By symmetry, the spins must fluctuate along the z axis; the insets show on which sites or bonds they reside. The even-parity states have a divergent pairing strength at the QCP, signaling strong triplet pairing. In contrast, the odd-parity state is not substantially enhanced near the QCP. The eigenvalues for spin fluctuation-induced pairing are much larger than those promoted by the corresponding LC fluctuations in Fig. 3. These spin eigenvalues will be reduced by the smallness of the spin-orbit coupling. For the triplet states $p \perp z$ and $p \parallel z$, the Balian-Werthamer vector Δ_a is oriented along the xy plane and the z axis, respectively.

gap function of the Bogoliubov–de Gennes Hamiltonian via $\Delta_{\sigma\sigma'}(\mathbf{p}) = \Delta_+(\mathbf{p})i\sigma_{\sigma\sigma'}^y$ for singlet and $\Delta_{\sigma\sigma'}(\mathbf{p}) = \Delta_-(\mathbf{p})(\sigma^a i\sigma^y)_{\sigma\sigma'}$ for triplet pairing, respectively. Here, all triplet orientations are degenerate because we assumed no spin-orbit coupling and purely orbital LCs $\Gamma_{\mathbf{k},\mathbf{p}} = \gamma_{\mathbf{k},\mathbf{p}} \otimes \sigma^0$.

The Cooper channel interactions are given by

$$V_{\pm}(\mathbf{p}, \mathbf{k}) = -\frac{1}{2} [V_0(\mathbf{p}, \mathbf{k}) \pm V_0(\mathbf{p}, -\mathbf{k})] \quad (3)$$

where the overall minus sign arises because LCs are odd under time reversal. $V_0(\mathbf{p}, \mathbf{k}) = g^2\chi(\mathbf{p} - \mathbf{k})f(\mathbf{p}, \mathbf{k})$ is a combination of the LC correlation function $\chi(\mathbf{q})$ and the matrix element

$$f(\mathbf{p}, \mathbf{k}) = |u_{\mathbf{p}}^\dagger \gamma_{\mathbf{p},\mathbf{k}} u_{\mathbf{k}}|^2 > 0 \quad (4)$$

where $u_{\mathbf{k}}$ are the orbital components of the conduction band eigenvectors. The $f(\mathbf{p}, \mathbf{k})$ contain information about the nature and symmetry of the LC state via the form factor $\gamma_{\mathbf{p},\mathbf{k}}$. For the coupling constant g , we assume a value that yields sufficiently small dimensionless eigenvalues λ .

Generic behavior near the QCP

Before we discuss our results near the QCP, let us briefly comment on pairing mediated by critical fluctuations of other order parameters. For order parameters that are spin-ferromagnetic or preserve time-reversal symmetry, as the QCP is approached ($r \rightarrow 0$), one finds that the largest eigenvalue of the gap equation diverges like $\lambda \propto r^{-\psi}$ with $\psi > 0$ (29, 36, 37), as schematically shown by the blue line in Fig. 1. While this corresponds to a breakdown of the weak-coupling analysis, it also signals the emergence of a strong pairing tendency near the QCP. Weak-coupling theory alone cannot determine the precise behavior in the immediate vicinity of the QCP, yet numerous computational approaches show that T_c is largest at or near the QCP (38–40). This is the much-discussed efficiency of quantum-critical pairing (41, 42). Following (29), the divergence of λ is based on the assumption that the forward-scattering contribution $f(\mathbf{p}, \mathbf{k})|_{\mathbf{p} \rightarrow \mathbf{k}}$ is attractive and varies smoothly as a function of

$\mathbf{q} = \mathbf{p} - \mathbf{k}$. Under these circumstances, the largest eigenvalue of the gap equation is given by

$$\lambda \approx \lambda_0 \int d^{d-1}q_{\parallel} \chi(\mathbf{q}_{\parallel}) \quad (5)$$

where \mathbf{q}_{\parallel} are the components of the transferred momentum \mathbf{q} tangential to the Fermi surface and $\lambda_0 = g^2 \langle v_{\mathbf{k}}^{-1} f(\mathbf{k}, \mathbf{k}) \rangle_{\text{FS}}$. Using the scaling form $\chi(\mathbf{q}_{\parallel}) = F(q_{\parallel}\xi) / q_{\parallel}^{2-\eta}$ introduced previously, the integral in Eq. 5 gives $\psi = (3 - d - \eta)\nu$ if $d < 3 - \eta$. Hence, QCPs in $d = 2$ with $\eta < 1$ yield strong pairing. In $d = 3$, the enhancement is logarithmic, provided $\eta = 0$.

For intra-unit-cell orbital magnetism, however, the analysis of the pairing enhancement at the QCP is different and depends on the parity p_{Φ} of the LC state. In Methods A, we show that

$$\begin{aligned} f(\mathbf{p}, \mathbf{k})|_{\mathbf{p} \rightarrow \mathbf{k}} &\propto (\mathbf{p} - \mathbf{k})^2 & \text{if } p_{\Phi} = +1, \\ f(\mathbf{p}, \mathbf{k})|_{\mathbf{p} \rightarrow \mathbf{k}} &\propto \text{const.} > 0 & \text{if } p_{\Phi} = -1 \end{aligned} \quad (6)$$

as well as $f(\mathbf{p}, \mathbf{k})|_{\mathbf{p} \rightarrow -\mathbf{k}} \propto (\mathbf{p} + \mathbf{k})^2$ for both values of p_{Φ} . Hence, for even-parity LCs ($p_{\Phi} = +1$), the forward-scattering singularity as $r \rightarrow 0$ originating from $\chi(\mathbf{p} - \mathbf{k})$ in Eq. 5 is eliminated for $d \geq 1 - \eta$ and suppressed for $d < 1 - \eta$ down to $\lambda \propto r^{(d-1+\eta)\nu}$. Thus, for $d \geq 1 - \eta$, which we expect to always be fulfilled for systems of interest, the pairing response is not enhanced near the QCP, as illustrated in Fig. 1 (orange line). For odd-parity LC ($p_{\Phi} = -1$), the implications of Eq. 6 are even more dramatic. The positive-definiteness of the matrix element $f(\mathbf{p}, \mathbf{k}) > 0$ when combined with the monotonous decay of $\chi(\mathbf{q})$ from its $\mathbf{q} = 0$ maximum implies that all pairing channels are repulsive near the QCP, diverging as $\propto -r^{-\psi}$ (green line in Fig. 1). Only away from the QCP can finite- \mathbf{q} features of the matrix element $f(\mathbf{p}, \mathbf{k})$ or the Fermi velocity $v_{\mathbf{k}}$ result in an attractive pairing channel that, however, is parametrically weak. This robust result does not depend on material details and is a consequence of the fact that LC order breaks time-reversal symmetry with a trivial form factor in spin space. Hence, for two-dimensional systems, even-parity intra-unit-cell LCs are inefficient

and odd-parity intra-unit-cell LCs are detrimental to pairing near their QCP.

Application to overdoped cuprates

The conclusions drawn so far are valid for generic systems. Now, we consider the cuprates. We analyze them from the far-overdoped side of the phase diagram where the normal state is a Fermi liquid (43–50). Provided the pairing state and dominant mechanism are unchanged across the phase diagram, this should give information about optimally doped systems as well. For the one-particle Hamiltonian H_0 , we use the well-established three-band tight-binding model (9, 51–55) that is based on the copper $3d_{x^2-y^2}$ and oxygen $2p_{x,y}$ orbitals (see Fig. 2A and Methods B). This model is characterized by the charge-transfer energy $\epsilon_d - \epsilon_p$ and the hopping amplitudes shown in Fig. 2A. We use the Cu-O hopping element $t_{pd} \approx 1.4\text{eV}$ to set the overall energy scale. Although we considered a wide range of tight-binding parameters discussed in the literature (56–60), the precise choice of tight-binding parameters has proven to have a minimal impact on our results. We thus use one representative choice of parameters (Methods B) throughout.

Interactions in the cuprates are most often modeled with extended Hubbard interactions. Whether LC order emerges in the resulting model is under debate, as there are computational investigations that do (59, 61, 62) and do not (63–65) find evidence for LCs. While these are important microscopic investigations, we take a more phenomenological perspective and assume from the outset that intra-unit-cell LC fluctuations exist and exploit the consequences of this assumption. In this phenomenological approach, we can independently vary the LC correlation length through r and the hole doping p through the chemical potential μ . In the real system, the two are not independent, something we must keep in mind when interpreting our results. For the LC correlation function, we use $\chi(\mathbf{q}) = \chi_0 \cdot 4/[2 + 2r - (1 - r)\nu_{\mathbf{q}}]$ where $\chi_0 > 0$ and $\nu_{\mathbf{q}} = \cos q_x + \cos q_y$; negative $\chi(\mathbf{q})$ indicate LC condensation. As we do not know in which LC channel the system orders, we classify all the possibilities (Fig. 2, B to D; Methods C) and study Cooper pairing for each. Figure 3 shows the results.

To classify intra-unit-cell LCs, we consider the minimal set of sites that maps onto itself under all point group operations, namely, the set made of one Cu site and the four surrounding O sites (see the blue-shaded region of Fig. 2A). The corresponding five-component spinor $a_{\mathbf{k}\sigma} = (d_{\mathbf{k}\sigma}, p_{x,\mathbf{k}\sigma}, p_{y,\mathbf{k}\sigma}, e^{-ik_x}p_{x,\mathbf{k}\sigma}, e^{-ik_y}p_{y,\mathbf{k}\sigma})^T$ has particularly simple symmetry transformation rules, facilitating the group-theoretic classification (Methods C). In total, there are 25 Hermitian matrices Λ that one may use to construct an orbital intra-unit-cell fermionic bilinear $\phi(\mathbf{R}) = \sum_{\sigma} a_{\sigma}^{\dagger}(\mathbf{R})\Lambda a_{\sigma}(\mathbf{R})$. By projecting onto the Bloch states via $a_{\mathbf{k}\sigma} = W_{\mathbf{k}}c_{\mathbf{k}\sigma}$ where $c_{\mathbf{k}\sigma} = (d_{\mathbf{k}\sigma}, p_{x,\mathbf{k}\sigma}, p_{y,\mathbf{k}\sigma})^T$, one finds the form factors $\gamma_{\mathbf{k}\mathbf{p}} = W_{\mathbf{k}}^{\dagger}\Lambda W_{\mathbf{p}}$ of Eq. 1. Since $W_{\mathbf{k}}^* = W_{-\mathbf{k}}$, the condition $\gamma_{\mathbf{k}\mathbf{p}}^* = -\gamma_{-\mathbf{k},-\mathbf{p}}$ implies that LCs have purely imaginary Λ . The purely imaginary nature of the orbital matrix Λ can be interpreted as introducing phase shifts in the bare hopping parameters of H_0 . Via a reverse Peierls substitution, these phase shifts correspond to magnetic fluxes generated by orbital currents.

There are in total $10 = 5(5 - 1)/2$ imaginary Hermitian matrices Λ . We chose them so that they transform under irreducible representations (irreps) of the tetragonal point group D_{4h} (66). These irreps, in turn, determine which additional crystallographic symmetries are broken (if any) by the LC, besides time reversal. The

explicit expressions of the LC Λ matrices are provided in Methods C. Upon enforcing the constraints that no global currents are allowed (1–3) and that the currents obey Kirchhoff's law at steady state, we are left with a total of six LC patterns (see Methods D). Of these six LC Λ , one is $g_{xy}(x^2-y^2)$ -wave, one is $d_{x^2-y^2}$ -wave, and two pairs are (p_x, p_y) -wave (see Fig. 2, B to D). The corresponding order parameters we shall call Φ_g , Φ_d , and $\Phi_p = (\Phi_{px}, \Phi_{py})$. As shown in Fig. 4, one may interpolate between the two p-wave options, which we parametrize with $\alpha \in [0, \pi]$. This follows from the existence of several paths connecting opposite oxygen orbitals of the same kind: an indirect path through the Cu atom (process c_1 in Fig. 4C), a direct path (process c_2), and an indirect path through the O atoms (process c_3). In the actual cuprate structure, the second process is mediated by the Cu:4s orbital (57, 58, 67). In Figs. 2D and 3, we use $\alpha = 0$. These LCs are essentially the same ones that were discussed in (7), with the exception of one LC state discussed therein that breaks translation invariance.

Using the form factors $\Gamma_{\mathbf{k}\mathbf{p}} = W_{\mathbf{k}}^{\dagger}\Lambda W_{\mathbf{p}} \otimes \sigma^0$ from the analysis above, we numerically solve the linearized gap (Eq. 2) supplemented by Eqs. 3 and 4. We consider two tuning parameters: the distance to the QCP r and the chemical potential μ . The latter determines the hole doping concentration p and the shape of the Fermi surface, which crosses the Van Hove singularity (VHS) at $p = 0.36$ (see inset of Fig. 3, D and E). All eigenvalues λ are measured in terms of the dimensionless parameter $g^2\chi_0/t_{pd}$ and are thus comparable. The results are shown in Fig. 3.

Φ_g describes a $g_{xy}(x^2-y^2)$ -wave LC, which gives rise to an orbital-magnetic dipole, i.e., an orbital ferromagnet. It has even parity ($p_{\Phi} = +1$) and transforms under the A_{2g} irrep of D_{4h} . Φ_g is an Ising order parameter and can be polarized by an external magnetic field oriented along the z direction B_z via the coupling $H_c = -\kappa \Phi_g B_z$, where κ is a coupling constant. As shown in Fig. 3A, Φ_g fluctuations result in weak d_{xy} pairing, which is weak in the sense that the pairing eigenvalue λ does not diverge at the QCP ($r \rightarrow 0$). This is in agreement with Eq. 6 and the general result discussed thereafter. There are sub-leading singlet and triplet instabilities as well. In Fig. 3D, one sees that the leading d_{xy} instability is weakly enhanced near the VHS, while $d_{x^2-y^2}$ pairing is strongly suppressed in the same limit. The reported (7) degeneracy between d_{xy} and $d_{x^2-y^2}$ pairing for Φ_g is recovered in the limit of extremely overdoped systems with small Fermi surfaces, $p \rightarrow 1$. The counterintuitive result that this degeneracy is lifted in favor of d_{xy} pairing by realistic μ values follows from the fact that the matrix element $f(\mathbf{p}, \mathbf{k})$ vanishes whenever either \mathbf{p} or \mathbf{k} are at the high-symmetry Van Hove points $(\pm\pi, 0)$ or $(0, \pm\pi)$, as proved in Methods C. Hence Φ_g -mediated pairing cannot exploit the enhanced density of states due to the VHS.

The order parameter Φ_d is associated with $d_{x^2-y^2}$ -wave LCs and is a magnetic octupole, i.e., an orbital altermagnet that is invariant under the combination of time reversal and a fourfold rotation about the z axis, $\Theta_{C_{4z}}\Phi_d = \Phi_d$. It transforms under the B_{1g} irrep, and as such, it has even parity, $p_{\Phi} = +1$. Like Φ_g , Φ_d is an Ising order parameter, but unlike Φ_g , it does not have a magnetic moment. Instead, it displays piezomagnetism and can be polarized by the combination of shear strain ϵ_{xy} and an external magnetic field pointing in the z direction: $H_c = -\kappa \Phi_d B_z \epsilon_{xy}$. As shown in Fig. 3B, Φ_d promotes weak $d_{x^2-y^2}$ pairing with several sub-leading singlet and one triplet pairing instabilities. The pairing strength of the leading $d_{x^2-y^2}$ channel is enhanced if one tunes the chemical potential to the VHS, as can be seen in Fig. 3E.

Finally, $\Phi_p = (\Phi_{px}, \Phi_{py})$ is a two-component order parameter that describes a p-wave LC, giving rise to a toroidal magnetic dipole moment. It transforms under the E_u irrep and thus has odd parity, $p_\Phi = -1$. Its statistical mechanics is governed by a four-state clock model, a result that follows from a Landau expansion that includes quartic terms. The four states for $\alpha = 0$, defined in Fig. 4, are shown in Fig. 2D. Φ_p has a magneto-electric response, that is to say, it can be polarized by crossed electric and magnetic fields according to $H_c = -\kappa(\Phi_{px}B_x + \Phi_{py}B_y)E_z$. A similar effect can be achieved by applying, instead of electric fields, time-varying currents along the z axis. As shown in Fig. 3C, away from the QCP, we find that Φ_p fluctuations result in weak extended s-wave superconductivity that is dominated by an angle-dependent gap function of the form $\Delta(\varphi) = \Delta_0 + \Delta_1 \cos(4\varphi)$ with $|\Delta_1| \gg |\Delta_0|$, yielding eight vertical line nodes. In addition, there is a sub-leading weak $d_{x^2-y^2}$ pairing state that could only become dominant if one could approach smaller hole doping values without increasing the LC correlation length (see Fig. 3F). Most importantly, and in complete agreement with the general discussion for odd-parity LC states after Eq. 6, the pairing eigenvalues turn strongly repulsive in all symmetry channels as one approaches the QCP, as signaled by the absence of any positive eigenvalue in Fig. 3C as $r \rightarrow 0$. While the results in Fig. 3 (C and F) refer to $\alpha = 0$, in Fig. 4A, we show the impact of the parameter α on pairing. Recall that α parametrizes the relative weights between different paths connecting opposite O orbitals (see Fig. 4, B and C). The impact is clearly minor, consisting of the emergence of other weak subleading states for a range of α values and of the suppression of the leading state near $\alpha = \pi/4$.

Our analysis so far has considered only pure orbital magnetism. Of course, in any system with spin-orbit coupling, spin fluctuations with the same symmetry as the LC patterns are expected to emerge (68, 69). Their pairing was analyzed with a generalization of Eq. 2 to spin exchange. The degeneracy between the in-plane and out-of-plane triplet channels is now lifted by the nontrivial spin structure. The results are shown in Fig. 5. For even-parity LC order, we find strong pairing in triplet channels that will eventually dominate as $r \rightarrow 0$ over the weak singlet instabilities discussed earlier. Conversely, for odd-parity LCs, spin fluctuations promote parametrically weak triplet pairing. Hence the strongly repulsive behavior of the pairing interaction in the orbital sector cannot be offset by the contribution from spin fluctuations. These results can, in fact, be derived from Eq. 6, adapted to spin-mediated pairing. The crucial difference is that the conditions for the two behaviors in Eq. 6 are interchanged: Now, forward scattering vanishes for odd parity ($p_\Phi = -1$).

DISCUSSION

In our analysis, we did not derive the existence of orbital magnetism or LCs. Instead, we started with the assumption that they exist and then explored the strength and type of superconductivity that they promote. We find that away from the associated QCP, intra-unit-cell LC fluctuations can give rise to unconventional pairing. Because of the negative-definiteness of the singlet Cooper channel interaction, $V_+(\mathbf{p}, \mathbf{k}) < 0$, any s-wave solution that has no nodes, $\Delta_+(\mathbf{k}) > 0$, necessarily has negative eigenvalues λ in Eq. 2. Hence, attractive pairing channels must be unconventional, if they exist. However, in distinction to pairing mediated by spin-magnetic (34, 35), nematic (29–31), or ferroelectric (32, 33) fluctuations, we do not find an enhancement of the pairing that is related to the vicinity of the

QCP. For even-parity LCs, the weak orbital pairing behavior persists near the QCP and, in the presence of spin-orbit coupling, is overwhelmed by the symmetry-equivalent spin fluctuation that favors triplet pairing. In contrast, odd-parity LCs near the QCP are strongly pair-breaking in all symmetry channels, a behavior that cannot be circumvented even when one allows for spin-orbit coupling and spin fluctuations. This behavior is consistent with the fact that in the ordered phase, a space-inversion and time-reversal symmetry breaking state would suppress the Cooper instability. Hence, critical intra-unit-cell odd-parity LCs behave analogously to photons, where the coupling of a fermion current to the vector potential—odd under parity and time reversal—yields no superconductivity either. Note that the absence of a strong attractive pairing interaction at the QCP justifies a posteriori the weak-coupling analysis used in this paper.

With regard to the cuprate superconductors, we have studied them in the far-overdoped regime where complications relating to Mott physics, the pseudogap, and competing orders can be neglected (70–72). We find that the odd-parity LC state Φ_p , which is the one most widely discussed in the cuprates, will at best give rise to extended s-wave pairing away from the QCP. As one approaches the QCP, Φ_p will not only fail to induce pairing in any channel but also suppress pairing that might arise from other collective modes.

In (7), it was argued that pairing is caused by fluctuations of the conjugate momentum of Φ_p and that this conjugate momentum has an essentially momentum-independent correlation function. The conjugate momentum of Φ_p must be odd under time reversal, even under parity, and transform like a magnetic dipole. Hence, it transforms like Φ_g and is governed by the same form factor. The analysis at the QCP is then formally identical to the case $r \sim 1$, where, as demonstrated in Fig. 3A, we find weak d_{xy} -wave pairing. We do not find the $d_{x^2-y^2}$ pairing state that was reported for fluctuations from Φ_g (7, 37). The reason is that the matrix element $f(\mathbf{p}, \mathbf{k}) \propto [(\mathbf{k} \times \mathbf{p}) \cdot \hat{\mathbf{z}}]^2$ used in (7, 37) was estimated in the continuum limit, which ignores the fact that $f(\mathbf{p}, \mathbf{k})$ vanishes when either \mathbf{p} or \mathbf{k} are at the high-symmetry Van Hove points $(\pi, 0)$ or $(0, \pi)$ (see Methods C). Φ_g therefore cannot take advantage of the high density of states near these Van Hove momenta. Only for chemical potentials that yield very small electron pockets do we retrieve the continuum limit matrix element and the degeneracy between d_{xy} and $d_{x^2-y^2}$ pairing that follows from it (7, 37) (see Fig. 3D). The continuum limit is fully consistent with Eq. 6 for $p_\Phi = +1$, i.e., it only gives rise to weak pairing near the QCP. While pairing due to the conjugate momentum is allowed and interesting, the order parameter itself should always couple directly to electrons and its much stronger pair-breaking tendency cannot, in our view, be ignored.

In conclusion, superconductivity due to this highly interesting state of matter is unlikely in general and in the cuprates in particular if we restrict ourselves to intra-unit-cell (i.e., $\mathbf{q} = 0$) ordering. It is an interesting question of whether this remains the case if LCs break additional translation symmetries, which has been proposed to take place in cuprates (73–77) and in kagome superconductors (24). For such staggered LCs, the Cooper channel interaction is again uniformly repulsive, $V_+(\mathbf{p}, \mathbf{k}) < 0$, but now with a peak at a finite momentum transfer \mathbf{Q} , a behavior known to give rise to unconventional superconductivity (78, 79). We find that such pairing due to staggered LCs strengthens as the QCP is approached as there are no generic symmetries, like parity or time-reversal, that suppress it. For the electronic structure of the cuprates, we obtain that d-wave

and p-wave LCs with $\mathbf{Q} = (\pi, \pi)$ both favor strong $d_{x^2-y^2}$ -wave pairing, whereas g-wave LCs do not because of the suppression of $f(\mathbf{p}, \mathbf{k})$ at the Van Hove points.

METHODS

A. LC exchange

The fully antisymmetrized interaction due to exchange of LC fluctuations that couple to the fermionic bilinear of Eq. 1 equals $U_{1234} = -(V_{1234} - V_{1243})$, where $i \equiv (\mathbf{k}_i, \alpha_i)$, α_i is the combined orbital and spin index, and

$$V_{1234} = g^2 \chi(\mathbf{k}_1 - \mathbf{k}_3) [\Gamma_{\mathbf{k}_1, \mathbf{k}_3}]_{\alpha_1 \alpha_3} [\Gamma_{\mathbf{k}_2, \mathbf{k}_4}]_{\alpha_2 \alpha_4} \quad (7)$$

See Fig. 6 for the diagram. The pairing instability is determined by the Cooper channel interaction $\tilde{V}_{\alpha_3 \alpha_4}^{\alpha_1 \alpha_2}(\mathbf{k}_1, \mathbf{k}_3) \equiv U_{\alpha_1 \alpha_2, \alpha_3 \alpha_4}(\mathbf{k}_1, -\mathbf{k}_1, \mathbf{k}_3, -\mathbf{k}_3)$ through the linearized gap equation (80, 81)

$$[\Delta_{\mathbf{p}}]_{\alpha_1 \alpha_2} = -\frac{1}{2N} \sum_{\mathbf{k} \alpha_3 \alpha_4} \tilde{V}_{\alpha_3 \alpha_4}^{\alpha_1 \alpha_2}(\mathbf{p}, \mathbf{k}) \sum_n \frac{\tanh \frac{1}{2} \beta \varepsilon_{\mathbf{k}n}}{2\varepsilon_{\mathbf{k}n}} [P_{\mathbf{k}n} \Delta_{\mathbf{k}} P_{-\mathbf{k}n}^T]_{\alpha_3 \alpha_4} \quad (8)$$

Here, n is the bands index, $\varepsilon_{\mathbf{k}n}$ is the band dispersion, and $P_{\mathbf{k}n} = \sum_s |u_{\mathbf{k}ns}\rangle \langle u_{\mathbf{k}ns}|$ projects onto the Bloch states of the band. The gap matrix was expressed in terms of a Balian-Werthamer vector $\Delta_a(\mathbf{p})$

$$[\Delta_{\mathbf{p}}]_{\alpha_1 \alpha_2} = \sum_{a=0}^3 \Delta_a(\mathbf{p}) \left[P_{\mathbf{p}}^a i\sigma^y \right]_{\alpha_1 \alpha_2} \quad (9)$$

where $P_{\mathbf{p}}^a = \sum_{ss'} u_{\mathbf{p}ns} \sigma_{ss'}^a u_{\mathbf{p}ns'}^\dagger$ for that n whose $\varepsilon_{\mathbf{p}n} = 0$. Projecting onto a single Fermi surface for purely orbital $\Gamma_{\mathbf{p}, \mathbf{k}} = \gamma_{\mathbf{p}, \mathbf{k}} \otimes \sigma^0$ under the assumption of no spin-orbit coupling yields the linearized gap Eq. 2.

The matrix element $f(\mathbf{p}, \mathbf{k}) = |u_{\mathbf{p}}^\dagger \gamma_{\mathbf{p}, \mathbf{k}} u_{\mathbf{k}}|^2$ of Eq. 4 may vanish for $\mathbf{p} = \pm \mathbf{k}$, depending on the parity and time-reversal sign of the order parameter (1). Under inversion symmetry $\gamma_{\mathbf{p}, \mathbf{k}} \xrightarrow{P} p_\Phi \gamma_{-\mathbf{p}, -\mathbf{k}}$, where p_Φ is the parity of Φ . Since LCs are odd under time-reversal, $\gamma_{\mathbf{p}, \mathbf{k}} \xrightarrow{\Theta} -\gamma_{-\mathbf{p}, -\mathbf{k}}^*$. If we further use the transformation properties of orbital Bloch functions $u_{\mathbf{k}} \xrightarrow{P} u_{-\mathbf{k}}^\dagger = u_{\mathbf{k}}^*$ under these same symmetries, we find

$$u_{\mathbf{k}}^\dagger \gamma_{\mathbf{k}, \mathbf{p}} u_{\mathbf{p}} = -p_\Phi u_{\mathbf{p}}^\dagger \gamma_{\mathbf{p}, \mathbf{k}} u_{\mathbf{k}} \quad (10)$$

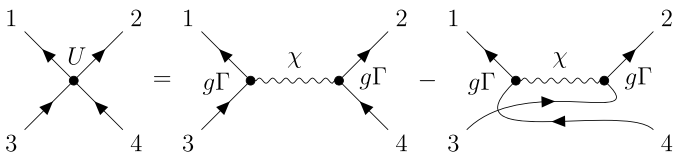


Fig. 6. Diagram of the antisymmetrized four-fermion interaction that is mediated by a bosonic collective mode. The bosonic propagator is denoted with a wavy line.

Hence, for even-parity ($p_\Phi = +1$) LCs, the matrix element $f(\mathbf{p}, \mathbf{k})$ vanishes at $\mathbf{p} = \mathbf{k}$, yielding Eq. 6. Because of time-reversal oddness of LCs, $u_{-\mathbf{k}}^\dagger \gamma_{-\mathbf{k}, -\mathbf{p}} u_{-\mathbf{p}} = -u_{\mathbf{p}}^\dagger \gamma_{\mathbf{p}, \mathbf{k}} u_{\mathbf{k}}$ so $f(-\mathbf{k}, \mathbf{k}) = 0$ also vanishes.

B. Electronic structure of cuprates

In cuprates, the states closest to the Fermi level primarily derive from anti-bonding hybridization between $\text{Cu}:3d_{x^2-y^2}$ orbitals and $\text{O}:2p_{x,y}$ orbitals oriented along the ligands (9, 56, 82, 83) (see Fig. 2A). These orbitals are the basis of the three-band tight-binding model (9, 51, 52, 53, 54, 55) that we use in our calculation. In the orbital basis $c_{\mathbf{k}\sigma} = (d_{\mathbf{k}\sigma}, p_{x, \mathbf{k}\sigma}, p_{y, \mathbf{k}\sigma})^T$, the three-band Hamiltonian takes the form

$$H_{\mathbf{k}} = \begin{pmatrix} h_d(\mathbf{k}) & h_{pd}(\mathbf{k}) & -h_{pd}(\tilde{\mathbf{k}}) \\ & h_p(\mathbf{k}) & h_{pp}(\mathbf{k}) \\ \text{c. c.} & & h_p(\tilde{\mathbf{k}}) \end{pmatrix} \quad (11)$$

where $\mathbf{k} = (k_x, k_y)$, $\tilde{\mathbf{k}} = (k_y, k_x)$, and

$$\begin{aligned} h_d(\mathbf{k}) &= \epsilon_d - \mu \\ h_p(\mathbf{k}) &= \epsilon_p + 2t'_{pp} \cos k_x - \mu \\ h_{pd}(\mathbf{k}) &= t_{pd}(1 - e^{-ik_x}) \\ h_{pp}(\mathbf{k}) &= -t_{pp}(1 - e^{ik_x})(1 - e^{-ik_y}) \end{aligned} \quad (12)$$

Typical values for the tight-binding parameters used in the literature are (60) ($\epsilon_d - \epsilon_p$)/ $t_{pd} \in [2.5, 3.5]$, $t_{pp}/t_{pd} \in [0.5, 0.6]$, and $t'_{pp}/t_{pd} \approx 0$, with $t_{pd} \in [1.2, 1.5]$ eV. t'_{pp} is not really negligible (57, 58, 67), although it is often assumed to be. The importance of t'_{pp} for LCs was emphasized in (59). We have considered eight different parameter sets that cover a wide range of physically reasonable possibilities (56–60) and that reproduce the ARPES Fermi surface shapes (47, 48, 84, 85). Our results have turned out to be insensitive to these changes in the one-particle Hamiltonian. All results shown or quoted in the paper are for the representative parameter set $\epsilon_d - \epsilon_p = 3t_{pd}$, $t_{pp} = 0.6t_{pd}$, $t'_{pp} = 0.5t_{pd}$, and $\mu = 0.9t_{pd}$, with $\epsilon_d = 0$.

C. Classification of fermionic bilinears

Because of the nontrivial Wyckoff positions of the oxygen atoms, some point group operations (e.g., 90° rotations and parity) map orbitals between different primitive unit cells. In momentum space, the corresponding unitary matrices therefore acquire \mathbf{k} -dependent phases. For classification purposes, it is more convenient if the orbital and momentum dependencies of the point group matrices do not mix. Instead of the three-component spinor $c_\sigma(\mathbf{R}) = [d_\sigma(\mathbf{R}), p_{x, \sigma}(\mathbf{R} + \hat{x}/2), p_{y, \sigma}(\mathbf{R} + \hat{y}/2)]^T$, we therefore use an extended five-component spinor $a_\sigma(\mathbf{R}) = [d_\sigma(\mathbf{R}), p_{x, \sigma}(\mathbf{R} + \hat{x}/2), p_{y, \sigma}(\mathbf{R} + \hat{y}/2), p_{x, \sigma}(\mathbf{R} - \hat{x}/2), p_{y, \sigma}(\mathbf{R} - \hat{y}/2)]^T$ that is related to the primitive spinor through $a_{\mathbf{k}\sigma} = W_{\mathbf{k}} c_{\mathbf{k}\sigma}$, where

$$W_{\mathbf{k}} = \begin{pmatrix} 1 & 0 & 0 \\ 0 & 1 & 0 \\ 0 & 0 & 1 \\ 0 & e^{-ik_x} & 0 \\ 0 & 0 & e^{-ik_y} \end{pmatrix} \quad (13)$$

The corresponding extended unit cell is shaded blue in Fig. 2A.

In the extended basis, point group transformation matrices no longer depend on \mathbf{k} . Hence, LCs are classified by imaginary Hermitian 5×5 matrices. In total, there are 10 linearly independent matrices, which we classify into irreps of the D_{4h} point group (66) below

$$\begin{aligned} \Lambda^{A_{1g}} &= \frac{1}{2} \begin{pmatrix} 0 & -i & i & i & -i \\ i & 0 & 0 & 0 & 0 \\ -i & 0 & 0 & 0 & 0 \\ -i & 0 & 0 & 0 & 0 \\ i & 0 & 0 & 0 & 0 \end{pmatrix}, & \Lambda^{A_{2g}} &= \frac{1}{2} \begin{pmatrix} 0 & 0 & 0 & 0 & 0 \\ 0 & 0 & -i & 0 & -i \\ 0 & i & 0 & i & 0 \\ 0 & 0 & -i & 0 & -i \\ 0 & i & 0 & i & 0 \end{pmatrix}, \\ \Lambda_1^{B_{1g}} &= \frac{1}{2} \begin{pmatrix} 0 & -i & -i & i & i \\ i & 0 & 0 & 0 & 0 \\ i & 0 & 0 & 0 & 0 \\ -i & 0 & 0 & 0 & 0 \\ -i & 0 & 0 & 0 & 0 \end{pmatrix}, & \Lambda_2^{B_{1g}} &= \frac{1}{2} \begin{pmatrix} 0 & 0 & 0 & 0 & 0 \\ 0 & 0 & i & 0 & -i \\ 0 & -i & 0 & i & 0 \\ 0 & 0 & -i & 0 & i \\ 0 & i & 0 & -i & 0 \end{pmatrix}, \\ \Lambda_{1,x}^{E_u} &= \frac{1}{\sqrt{2}} \begin{pmatrix} 0 & -i & 0 & -i & 0 \\ i & 0 & 0 & 0 & 0 \\ 0 & 0 & 0 & 0 & 0 \\ i & 0 & 0 & 0 & 0 \\ 0 & 0 & 0 & 0 & 0 \end{pmatrix}, & \Lambda_{1,y}^{E_u} &= \frac{1}{\sqrt{2}} \begin{pmatrix} 0 & 0 & i & 0 & i \\ 0 & 0 & 0 & 0 & 0 \\ -i & 0 & 0 & 0 & 0 \\ 0 & 0 & 0 & 0 & 0 \\ -i & 0 & 0 & 0 & 0 \end{pmatrix}, \\ \Lambda_{2,x}^{E_u} &= \begin{pmatrix} 0 & 0 & 0 & 0 & 0 \\ 0 & 0 & 0 & -i & 0 \\ 0 & 0 & 0 & 0 & 0 \\ 0 & i & 0 & 0 & 0 \\ 0 & 0 & 0 & 0 & 0 \end{pmatrix}, & \Lambda_{2,y}^{E_u} &= \begin{pmatrix} 0 & 0 & 0 & 0 & 0 \\ 0 & 0 & 0 & 0 & 0 \\ 0 & 0 & 0 & -i & 0 \\ 0 & 0 & 0 & 0 & 0 \\ 0 & 0 & i & 0 & 0 \end{pmatrix}, \\ \Lambda_{3,x}^{E_u} &= \frac{1}{2} \begin{pmatrix} 0 & 0 & 0 & 0 & 0 \\ 0 & 0 & i & 0 & -i \\ 0 & -i & 0 & -i & 0 \\ 0 & 0 & i & 0 & -i \\ 0 & i & 0 & i & 0 \end{pmatrix}, & \Lambda_{3,y}^{E_u} &= \frac{1}{2} \begin{pmatrix} 0 & 0 & 0 & 0 & 0 \\ 0 & 0 & -i & 0 & -i \\ 0 & i & 0 & -i & 0 \\ 0 & 0 & i & 0 & i \\ 0 & i & 0 & -i & 0 \end{pmatrix} \end{aligned}$$

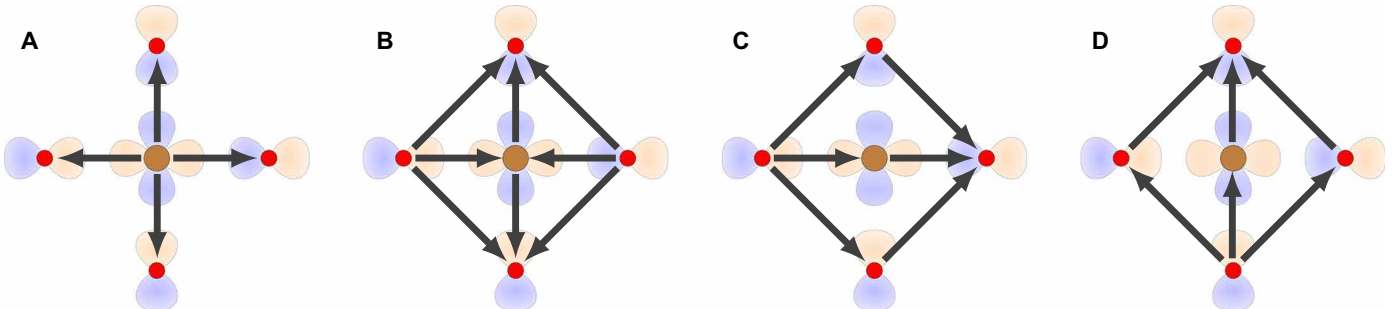


Fig. 7. LC patterns that violate Bloch and Kirchhoff constraints. (A and B) Local currents that would result in an accumulation of charge on d and p_y orbitals, respectively. (C and D) Global currents that would violate Bloch's theorem.

These matrices determine the form factors of the LC order parameter (Eq. 1) via $\Gamma_{\mathbf{k},\mathbf{p}} = W_{\mathbf{k}}^\dagger \Lambda W_{\mathbf{p}} \otimes \sigma^0$. Hence, one would expect a total of 10 possible LC states. In the next section, we show that charge conservation and the fact that spontaneous global currents are forbidden in purely electronic systems reduce the total number down to six.

The enhanced density of states near the Van Hove points $\mathbf{k}_X = (\pi, 0)$ and $\mathbf{k}_Y = (0, \pi)$ can be important for pairing. This turns out to not be the case for Φ_g -mediated pairing associated with A_{2g} LCs. To see why, let us consider \mathbf{k}_X . Parity implies that the band Hamiltonian is block-diagonal at this momentum, with the even-parity (d, p_x) block decoupled from odd-parity p_y . Since the conduction band state $u_{\mathbf{k}_X}$ has even parity and the g -wave LCs only couple the p_x and p_y orbitals, the relevant matrix element is $u_{\mathbf{k}_X}^\dagger W_{\mathbf{k}_X}^\dagger \Lambda^{A_{2g}} W_{\mathbf{p}} u_y$ where $u_y = (0, 0, 1)$. Let M be the mirror operation across the yz plane. Both the \mathbf{k}_X states and the p_y orbitals are even under M . The A_{2g} LCs are mirror-odd, however, making the matrix element vanish

$$\begin{aligned} u_{\mathbf{k}_X}^\dagger W_{\mathbf{k}_X}^\dagger \Lambda^{A_{2g}} W_{\mathbf{p}} u_y &= u_{\mathbf{k}_X}^\dagger W_{\mathbf{k}_X}^\dagger M^\dagger \Lambda^{A_{2g}} M W_{\mathbf{p}} u_y \\ &= -u_{\mathbf{k}_X}^\dagger W_{\mathbf{k}_X}^\dagger \Lambda^{A_{2g}} W_{\mathbf{p}} u_y = 0 \end{aligned} \quad (14)$$

The Van Hove point is therefore decoupled from the rest of the Fermi surface so there is no divergence at the Van Hove filling in Fig. 3D.

We recover the matrix element

$$u_{\mathbf{k}}^\dagger W_{\mathbf{k}}^\dagger \Lambda^{A_{2g}} W_{\mathbf{p}} u_{\mathbf{p}} = ic_0 \hat{\mathbf{z}} \cdot (\mathbf{k} \times \mathbf{p}) \quad (15)$$

of (7, 37) only when both \mathbf{p} and \mathbf{k} are near the Γ point, i.e., when the Fermi surface forms a small electron pocket at very large overdoping ($p \rightarrow 1$). For the coefficient, we find $c_0 = 2t_{pd}^2 / (\epsilon_d - \epsilon_p - 2t'_{pp})^2$.

D. Bloch and Kirchhoff constraints

An LC state is allowed only if its ordered state is consistent with the continuity equation (Kirchhoff's law) and with the Bloch constraint (1-3) that no global current can flow (see Fig. 7). A microscopic theory that properly derives such a state would naturally obey these conditions. In our phenomenological treatment, we must impose these constraints explicitly.

Bloch constraints: Using the extended basis, the global current operator can be written as

$$\mathbf{j} = \frac{1}{N} \sum_{\mathbf{R}ij} a_{i\alpha}^\dagger(\mathbf{R}) \mathbf{J}_{ij} a_{j\alpha}(\mathbf{R}) \quad (16)$$

Here, i, j are orbital indices and $(\mathbf{J})_{ij} = -i(\mathbf{r}_i - \mathbf{r}_j)t_{ij}$, where \mathbf{r}_i are the lattice vectors of the five extended unit cell atoms. The current matrix \mathbf{J} can be expressed in terms of time-reversal-odd E_u matrices

$$J_w = -\frac{1}{\sqrt{2}} t_{pd} \Lambda_{1,w}^{E_u} + t'_{pp} \Lambda_{2,w}^{E_u} + t_{pp} \Lambda_{3,w}^{E_u} \quad (17)$$

where $w = x$ or y . Hence, a finite global current can only be induced by p-wave LC order that transforms under the same E_u irrep. Consider a small, but finite, order parameter Φ_p that couples to fermions through the linear combination of form factors

$$\Gamma_{\mathbf{k},\mathbf{p}} = W_{\mathbf{k}}^\dagger \left(c_1 \Lambda_{1,w}^{E_u} + c_2 \Lambda_{2,w}^{E_u} + c_3 \Lambda_{3,w}^{E_u} \right) W_{\mathbf{p}} \quad (18)$$

Linear response theory then yields the constraint

$$\frac{\delta \langle j_w \rangle}{\delta \Phi_{p,w}} = -g \mathbf{h} \cdot \mathbf{c} = 0 \quad (19)$$

where $\mathbf{h} = (h_1, h_2, h_3)$ are the linear response coefficients obtained by evaluating the current expectation value and $\mathbf{c} = (c_1, c_2, c_3)$ specify the bilinear (18). $\mathbf{h}/|\mathbf{h}|$ depends weakly on chemical potential and for $\mu = 0.9t_{pd}$ equals $(0.85, 0.31, -0.43)$. After enforcing the above constraint, a one-parameter family of E_u bilinears $\mathbf{c} = \hat{\mathbf{h}}_c \cos(\alpha) + \hat{\mathbf{h}}_s \sin(\alpha)$ remains. Here, $\mathbf{h}_c = \mathbf{h} \times (0, 1, 0)$, $\hat{\mathbf{h}}_c = \mathbf{h}_c / |\mathbf{h}_c|$, $\mathbf{h}_s = \mathbf{h} \times \mathbf{h}_c$, and $\hat{\mathbf{h}}_s = \mathbf{h}_s / |\mathbf{h}_s|$.

Kirchhoff constraints: Local charge conservation entails that $\dot{n}_i = \sum_j G_{ij}$, where n_i is the charge on site i and $G_{ij} = -G_{ji}$ is the current flowing from site j to i . For a steady state, it must hold that $\langle \dot{n}_i \rangle = 0$. One easily finds that $G^{A_{1g}} = 2t_{pd}\Lambda_6^{A_{1g}}$ currents change the copper n_d and total oxygen $n_{px} + n_{py}$ charge, whereas $G^{B_{1g}} = -2t_{pd}\Lambda_4^{B_{1g}} + 4t_{pp}\Lambda_5^{B_{1g}}$ currents change $n_{px} - n_{py}$. Hence, currents associated with $G^{A_{1g}}$ and $G^{B_{1g}}$ must vanish. This implies that there cannot be an LC of A_{1g} symmetry and that the two coefficients c_1 and c_2 in the bilinear

$$\Gamma_{\mathbf{k},\mathbf{p}} = W_{\mathbf{k}}^\dagger \left(c_1 \Lambda_1^{B_{1g}} + c_2 \Lambda_2^{B_{1g}} \right) W_{\mathbf{p}} \quad (20)$$

are not independent. For $\mu = 0.9t_{pd}$, we find that $c_1/c_2 = 0.72$; this ratio depends weakly on μ .

REFERENCES AND NOTES

- D. Bohm, Note on a theorem of Bloch concerning possible causes of superconductivity. *Phys. Rev.* **75**, 502–504 (1949).
- Y. Ohashi, T. Momoi, On the Bloch theorem concerning spontaneous electric current. *J. Phys. Soc. Jpn.* **65**, 3254–3259 (1996).
- H. Watanabe, Bloch theorem in the presence of an additional conserved charge. *Phys. Rev. Res.* **4**, 013043 (2022).
- C. M. Varma, Non-Fermi-liquid states and pairing instability of a general model of copper oxide metals. *Phys. Rev. B* **55**, 14554–14580 (1997).
- M. E. Simon, C. M. Varma, Symmetry considerations for the detection of second-harmonic generation in cuprates in the pseudogap phase. *Phys. Rev. B* **67**, 054511 (2003).
- C. M. Varma, Theory of the pseudogap state of the cuprates. *Phys. Rev. B* **73**, 155113 (2006).
- V. Aji, A. Shekhter, C. M. Varma, Theory of the coupling of quantum-critical fluctuations to fermions and d -wave superconductivity in cuprates. *Phys. Rev. B* **81**, 064515 (2010).
- V. Aji, C. M. Varma, Spin order accompanying loop-current order in cuprate superconductors. *Phys. Rev. B* **75**, 224511 (2007).
- C. Varma, S. Schmitt-Rink, E. Abrahams, Charge transfer excitations and superconductivity in “ionic” metals. *Solid State Commun.* **62**, 681–685 (1987).
- B. Fauqué, Y. Sidis, V. Hinkov, S. Pailhès, C. T. Lin, X. Chaud, P. Bourges, Magnetic order in the pseudogap phase of high-Tc superconductors. *Phys. Rev. Lett.* **96**, 197001 (2006).
- H. A. Mook, Y. Sidis, B. Fauqué, V. Balédent, P. Bourges, Observation of magnetic order in a superconducting $\text{YBa}_2\text{Cu}_3\text{O}_{6.6}$ single crystal using polarized neutron scattering. *Phys. Rev. B* **78**, 020506 (2008).
- Y. Li, V. Balédent, N. Barišič, Y. Cho, B. Fauqué, Y. Sidis, G. Yu, X. Zhao, P. Bourges, M. Greven, Unusual magnetic order in the pseudogap region of the superconductor $\text{HgBa}_2\text{CuO}_{4+\delta}$. *Nature* **455**, 372–375 (2008).
- Y. Li, V. Balédent, G. Yu, N. Barišič, K. Hradil, R. A. Mole, Y. Sidis, P. Steffens, X. Zhao, P. Bourges, M. Greven, Hidden magnetic excitation in the pseudogap phase of a high-T(c) superconductor. *Nature* **468**, 283–285 (2010).
- P. Bourges, D. Bounoua, Y. Sidis, Loop currents in quantum matter. *C. R. Phys.* **22**, 7–31 (2021).
- T. P. Croft, E. Blackburn, J. Kulda, R. Liang, D. A. Bonn, W. N. Hardy, S. M. Hayden, No evidence for orbital loop currents in charge-ordered $\text{YBa}_2\text{Cu}_3\text{O}_{6+x}$ from polarized neutron diffraction. *Phys. Rev. B* **96**, 214504 (2017).
- A. M. Mounce, S. Oh, J. A. Lee, W. P. Halperin, A. P. Reyes, P. L. Kuhns, M. K. Chan, C. Dorow, L. Ji, D. Xia, X. Zhao, M. Greven, Absence of static loop-current magnetism at the apical oxygen site in $\text{HgBa}_2\text{CuO}_{4+\delta}$ from NMR. *Phys. Rev. Lett.* **111**, 187003 (2013).
- T. Wu, H. Mayaffre, S. Krämer, M. Horvatič, C. Berthier, W. Hardy, R. Liang, D. Bonn, M.-H. Julien, Incipient charge order observed by NMR in the normal state of $\text{YBa}_2\text{Cu}_3\text{O}_y$. *Nat. Commun.* **6**, 6438 (2015).
- S. Lederer, S. A. Kivelson, Observable NMR signal from circulating current order in YBCO. *Phys. Rev. B* **85**, 155130 (2012).
- S. Gheidi, K. Akintola, A. C. Y. Fang, S. Sundar, A. M. Côté, S. R. Dunsiger, G. D. Gu, J. E. Sonier, Absence of μSR evidence for magnetic order in the pseudogap phase of $\text{Bi}_{2-x}\text{Sr}_x\text{CaCu}_2\text{O}_{8+\delta}$. *Phys. Rev. B* **101**, 184511 (2020).
- Z. Zhu, J. Zhang, Z. Ding, C. Tan, C. Chen, Q. Wu, Y. Yang, O. O. Bernal, P.-C. Ho, G. D. Morris et al., Muon spin relaxation and fluctuating magnetism in the pseudogap phase of $\text{YBa}_2\text{Cu}_3\text{O}_y$. *Phys. Rev. B* **103**, 134426 (2021).
- L. Zhao, D. H. Torchinsky, H. Chu, V. Ivanov, R. Lifshitz, R. Flint, T. Qi, G. Cao, D. Hsieh, Evidence of an odd-parity hidden order in a spin-orbit coupled correlated iridate. *Nat. Phys.* **12**, 32–36 (2016).
- Y. J. Yan, M. Q. Ren, H. C. Xu, B. P. Xie, R. Tao, H. Y. Choi, N. Lee, Y. J. Choi, T. Zhang, D. L. Feng, Electron-doped Sr_2IrO_4 : An analogue of hole-doped cuprate superconductors demonstrated by scanning tunneling microscopy. *Phys. Rev. X* **5**, 041018 (2015).
- Y. K. Kim, N. H. Sung, J. D. Denlinger, B. J. Kim, Observation of a d -wave gap in electron-doped Sr_2IrO_4 . *Nat. Phys.* **12**, 37–41 (2016).
- C. Mielke, D. Das, J.-X. Yin, H. Liu, R. Gupta, Y.-X. Jiang, M. Medarde, X. Wu, H. C. Lei, J. Chang, P. Dai, Q. Si, H. Miao, R. Thomale, T. Neupert, Y. Shi, R. Khasanov, M. Z. Hasan, H. Luetkens, Z. Guguchia, Time-reversal symmetry-breaking charge order in a kagome superconductor. *Nature* **602**, 245–250 (2022).
- K. Sun, E. Fradkin, Time-reversal symmetry breaking and spontaneous anomalous Hall effect in Fermi fluids. *Phys. Rev. B* **78**, 245122 (2008).
- E. V. Castro, A. G. Grushin, B. Valenzuela, M. A. H. Vozmediano, A. Cortijo, F. de Juan, Topological Fermi liquids from Coulomb interactions in the doped honeycomb lattice. *Phys. Rev. Lett.* **107**, 106402 (2011).
- S. Sur, S.-S. Gong, K. Yang, O. Vafek, Quantum anomalous Hall insulator stabilized by competing interactions. *Phys. Rev. B* **98**, 125144 (2018).
- M. S. Scheurer, S. Sachdev, Orbital currents in insulating and doped antiferromagnets. *Phys. Rev. B* **98**, 235126 (2018).
- S. Lederer, Y. Schattner, E. Berg, S. A. Kivelson, Enhancement of superconductivity near a nematic quantum critical point. *Phys. Rev. Lett.* **114**, 097001 (2015).
- S. Lederer, Y. Schattner, E. Berg, S. A. Kivelson, Superconductivity and non-Fermi liquid behavior near a nematic quantum critical point. *Proc. Natl. Acad. Sci. U.S.A.* **114**, 4905–4910 (2017).
- A. Klein, A. Chubukov, Superconductivity near a nematic quantum critical point: Interplay between hot and lukewarm regions. *Phys. Rev. B* **98**, 220501 (2018).
- V. Kozii, L. Fu, Odd-parity superconductivity in the vicinity of inversion symmetry breaking in spin-orbit-coupled systems. *Phys. Rev. Lett.* **115**, 207002 (2015).
- A. Klein, V. Kozii, J. Ruhman, R. M. Fernandes, Theory of criticality for quantum ferroelectric metals. *Phys. Rev. B* **107**, 165110 (2023).
- R. Roussev, A. J. Millis, Quantum critical effects on transition temperature of magnetically mediated p -wave superconductivity. *Phys. Rev. B* **63**, 140504 (2001).
- A. V. Chubukov, A. M. Finkel’stein, R. Haslinger, D. K. Morr, First-order superconducting transition near a ferromagnetic quantum critical point. *Phys. Rev. Lett.* **90**, 077002 (2003).
- A. Abanov, A. V. Chubukov, J. Schmalian, Quantum-critical superconductivity in underdoped cuprates. *Europhys. Lett.* **55**, 369–375 (2001).

37. C. M. Varma, Considerations on the mechanisms and transition temperatures of superconductivity induced by electronic fluctuations. *Rep. Prog. Phys.* **75**, 052501 (2012).
38. X. Wang, Y. Schattner, E. Berg, R. M. Fernandes, Superconductivity mediated by quantum critical antiferromagnetic fluctuations: The rise and fall of hot spots. *Phys. Rev. B* **95**, 174520 (2017).
39. X. Y. Xu, K. Sun, Y. Schattner, E. Berg, Z. Y. Meng, Non-Fermi liquid at (2+1)-D ferromagnetic quantum critical point. *Phys. Rev. X* **7**, 031058 (2017).
40. X. Y. Xu, A. Klein, K. Sun, A. V. Chubukov, Z. Y. Meng, Identification of non-Fermi liquid fermionic self-energy from quantum Monte Carlo data. *npj Quantum Mater.* **5**, 65 (2020).
41. A. Abanov, A. V. Chubukov, Interplay between superconductivity and non-Fermi liquid at a quantum critical point in a metal. I. the γ model and its phase diagram at $T=0$: The case $0 < \gamma < 1$. *Phys. Rev. B* **102**, 024524 (2020).
42. Y.-M. Wu, A. Abanov, Y. Wang, A. V. Chubukov, Interplay between superconductivity and non-Fermi liquid at a quantum critical point in a metal. II. the γ model at a finite T for $0 < \gamma < 1$. *Phys. Rev. B* **102**, 024525 (2020).
43. C. Proust, E. Boaknin, R. W. Hill, L. Taillefer, A. P. Mackenzie, Heat transport in a strongly overdoped cuprate: Fermi liquid and a pure d-wave BCS superconductor. *Phys. Rev. Lett.* **89**, 147003 (2002).
44. S. Nakamae, K. Behnia, N. Mangkorntong, M. Nohara, H. Takagi, S. J. C. Yates, N. E. Hussey, Electronic ground state of heavily overdoped nonsuperconducting $\text{La}_{2-x}\text{Sr}_x\text{CuO}_4$. *Phys. Rev. B* **68**, 100502 (2003).
45. N. E. Hussey, M. Abdel-Jawad, A. Carrington, A. P. Mackenzie, L. Balicas, A coherent three-dimensional Fermi surface in a high-transition-temperature superconductor. *Nature* **425**, 814–817 (2003).
46. A. Damascelli, Z. Hussain, Z.-X. Shen, Angle-resolved photoemission studies of the cuprate superconductors. *Rev. Mod. Phys.* **75**, 473–541 (2003).
47. B. Plate, J. D. F. Mottershead, I. S. Elfimov, D. C. Peets, R. Liang, D. A. Bonn, W. N. Hardy, S. Chiuzaiba, M. Falub, M. Shi, L. Patthey, A. Damascelli, Fermi surface and quasiparticle excitations of overdoped $\text{Tl}_2\text{Ba}_2\text{CuO}_{6+\delta}$. *Phys. Rev. Lett.* **95**, 077001 (2005).
48. M. Horio, K. Hauser, Y. Sassa, Z. Mingazheva, D. Sutter, K. Kramer, A. Cook, E. Nocerino, O. K. Forslund, O. Tjernberg, M. Kobayashi, A. Chikina, N. B. M. Schröter, J. A. Krieger, T. Schmitt, V. N. Strocov, S. Pyon, T. Takayama, H. Takagi, O. J. Lipscombe, S. M. Hayden, M. Ishikado, H. Eisaki, T. Neupert, M. Mansson, C. E. Matt, J. Chang, Three-dimensional Fermi surface of overdoped La-based cuprates. *Phys. Rev. Lett.* **121**, 077004 (2018).
49. B. Vignolle, A. Carrington, R. A. Cooper, M. M. J. French, A. P. Mackenzie, C. Jaudet, D. Vignolles, C. Proust, N. E. Hussey, Quantum oscillations in an overdoped high-Tc superconductor. *Nature* **455**, 952–955 (2008).
50. A. F. Bangura, P. M. C. Rourke, T. M. Benson, M. Matusiak, J. R. Cooper, N. E. Hussey, A. Carrington, Fermi surface and anisotropy of the overdoped cuprate superconductor $\text{Tl}_2\text{Ba}_2\text{CuO}_{6+\delta}$ as revealed by quantum oscillations. *Phys. Rev. B* **82**, 140501 (2010).
51. V. J. Emery, Theory of high-Tc superconductivity in oxides. *Phys. Rev. Lett.* **58**, 2794–2797 (1987).
52. V. J. Emery, G. Reiter, Mechanism for high-temperature superconductivity. *Phys. Rev. B* **38**, 4547–4556 (1988).
53. P. B. Littlewood, C. M. Varma, E. Abrahams, Pairing instabilities of the extended Hubbard model for Cu–O–Based superconductors. *Phys. Rev. Lett.* **63**, 2602–2605 (1989).
54. Y. B. Gaididei, V. M. Loktev, On a theory of the electronic spectrum and magnetic properties of high-Tc superconductors. *Phys. Status Solidi B* **147**, 307–319 (1988).
55. R. T. Scalettar, D. J. Scalapino, R. L. Sugar, S. R. White, Antiferromagnetic, charge-transfer, and pairing correlations in the three-band Hubbard model. *Phys. Rev. B* **44**, 770–781 (1991).
56. W. E. Pickett, Electronic structure of the high-temperature oxide superconductors. *Rev. Mod. Phys.* **61**, 433–512 (1989).
57. E. Pavarini, I. Dasgupta, T. Saha-Dasgupta, O. Jepsen, O. K. Andersen, Band-structure trend in hole-doped cuprates and correlation with $T(c \text{ max})$. *Phys. Rev. Lett.* **87**, 047003 (2001).
58. P. R. C. Kent, T. Saha-Dasgupta, O. Jepsen, O. K. Andersen, A. Macridin, T. A. Maier, M. Jarrell, T. C. Schulthess, Combined density functional and dynamical cluster quantum Monte Carlo calculations of the three-band Hubbard model for hole-doped cuprate superconductors. *Phys. Rev. B* **78**, 035132 (2008).
59. C. Weber, T. Giamarchi, C. M. Varma, Phase diagram of a three-orbital model for high-Tc cuprate superconductors. *Phys. Rev. Lett.* **112**, 117001 (2014).
60. R. Photopoulos, R. Frésard, A 3D tight-binding model for La-based cuprate superconductors. *Ann. Phys.* **531**, 1900177 (2019).
61. C. Weber, A. Läuchli, F. Mila, T. Giamarchi, Orbital currents in extended Hubbard models of high-Tc cuprate superconductors. *Phys. Rev. Lett.* **102**, 017005 (2009).
62. R. Tazai, Y. Yamakawa, H. Kontani, Emergence of charge loop current in the geometrically frustrated Hubbard model: A functional renormalization group study. *Phys. Rev. B* **103**, L161112 (2021).
63. M. Greiter, R. Thomale, No evidence for spontaneous orbital currents in numerical studies of three-band models for the CuO planes of high temperature superconductors. *Phys. Rev. Lett.* **99**, 027005 (2007).
64. R. Thomale, M. Greiter, Numerical analysis of three-band models for CuO planes as candidates for a spontaneous T-violating orbital current phase. *Phys. Rev. B* **77**, 094511 (2008).
65. Y. F. Kung, C.-C. Chen, B. Moritz, S. Johnston, R. Thomale, T. P. Devereaux, Numerical exploration of spontaneous broken symmetries in multiorbital Hubbard models. *Phys. Rev. B* **90**, 224507 (2014).
66. M. S. Dresselhaus, G. Dresselhaus, A. Jorio, *Group Theory: Application to the Physics of Condensed Matter* (Springer, 2008).
67. O. Andersen, A. Liechtenstein, O. Jepsen, F. Paulsen, LDA energy bands, low-energy Hamiltonians, t' , t'' , $t_1(\mathbf{k})$, and J_{\perp} . *J. Phys. Chem. Solids* **56**, 1573–1591 (1995).
68. M. Klug, J. Kang, R. M. Fernandes, J. Schmalian, Orbital loop currents in iron-based superconductors. *Phys. Rev. B* **97**, 155130 (2018).
69. M. H. Christensen, T. Birol, B. M. Andersen, R. M. Fernandes, Loop currents in AV_3Sb_5 kagome metals: Multipolar and toroidal magnetic orders. *Phys. Rev. B* **106**, 144504 (2022).
70. K. P. Kramer, M. Horio, S. S. Tsirkin, Y. Sassa, K. Hauser, C. E. Matt, D. Sutter, A. Chikina, N. B. M. Schröter, J. A. Krieger, T. Schmitt, V. N. Strocov, N. C. Plumb, M. Shi, S. Pyon, T. Takayama, H. Takagi, T. Adachi, T. Ohgi, T. Kawamata, Y. Koike, T. Kondo, O. J. Lipscombe, S. M. Hayden, M. Ishikado, H. Eisaki, T. Neupert, J. Chang, Band structure of overdoped cuprate superconductors: Density functional theory matching experiments. *Phys. Rev. B* **99**, 224509 (2019).
71. N. R. Lee-Hone, H. U. Özdemir, V. Mishra, D. M. Broun, P. J. Hirschfeld, Low energy phenomenology of the overdoped cuprates: Viability of the Landau-BCS paradigm. *Phys. Rev. Res.* **2**, 013228 (2020).
72. T. A. Maier, S. Karakuzu, D. J. Scalapino, Overdoped end of the cuprate phase diagram. *Phys. Rev. Res.* **2**, 033132 (2020).
73. S. Chakravarty, R. B. Laughlin, D. K. Morr, C. Nayak, Hidden order in the cuprates. *Phys. Rev. B* **63**, 094503 (2001).
74. C. M. Varma, L. Zhu, Specific heat and sound velocity at the relevant competing phase of high-temperature superconductors. *Proc. Natl. Acad. Sci. U.S.A.* **112**, 6331–6335 (2015).
75. C. M. Varma, Pseudogap and Fermi arcs in underdoped cuprates. *Phys. Rev. B* **99**, 224516 (2019).
76. D. Bounoua, Y. Sidis, T. Loew, F. Bourdarot, M. Boehm, P. Steffens, L. Mangin-Thro, V. Balédun, P. Bourges, Hidden magnetic texture in the pseudogap phase of high-Tc $\text{YBa}_2\text{Cu}_3\text{O}_{6.6}$. *Commun. Phys.* **5**, 268 (2022).
77. D. Bounoua, Y. Sidis, M. Boehm, P. Steffens, T. Loew, L. S. Guo, J. Qian, X. Yao, P. Bourges, Universality of the $\mathbf{q}=1/2$ orbital magnetism in the pseudogap phase of the high-Tc superconductor $\text{YBa}_2\text{Cu}_3\text{O}_{6+x}$. *Phys. Rev. B* **108**, 214408 (2023).
78. D. J. Scalapino, The case for $d - x^2 - y^2$ pairing in the cuprate superconductors. *Phys. Rep.* **250**, 329–365 (1995).
79. S. Maiti, A. V. Chubukov, Superconductivity from repulsive interaction. *AIP Conf. Proc.* **1550**, 3–73 (2013).
80. A. J. Leggett, *Quantum Liquids: Bose Condensation and Cooper Pairing in Condensed-Matter Systems* (Oxford Univ. Press, 2006).
81. M. Sigrist, Introduction to unconventional superconductivity. *AIP Conf. Proc.* **789**, 165–243 (2005).
82. E. Dagotto, Correlated electrons in high-temperature superconductors. *Rev. Mod. Phys.* **66**, 763–840 (1994).
83. E. Pellegrin, N. Nücker, J. Fink, S. L. Molodtsov, A. Gutiérrez, E. Navas, O. Strelbe, Z. Hu, M. Domke, G. Kaindl, S. Uchida, Y. Nakamura, J. Markl, M. Klauda, G. Saemann-Ischenko, A. Krol, J. L. Peng, Z. Y. Li, R. L. Greene, Orbital character of states at the Fermi level in $\text{La}_{2-x}\text{Sr}_x\text{CuO}_4$ and $\text{R}_{2-x}\text{Ce}_x\text{CuO}_4$ (R=Nd,Sm). *Phys. Rev. B* **47**, 3354–3367 (1993).
84. T. Yoshida, X. J. Zhou, K. Tanaka, W. L. Yang, Z. Hussain, Z.-X. Shen, A. Fujimori, S. Sahrakorpi, M. Lindroos, R. S. Markiewicz, A. Bansil, S. Komiya, Y. Ando, H. Eisaki, T. Kakeshita, S. Uchida, Systematic doping evolution of the underlying Fermi surface of $\text{La}_{2-x}\text{Sr}_x\text{CuO}_4$. *Phys. Rev. B* **74**, 224510 (2006).
85. D. C. Peets, J. D. F. Mottershead, B. Wu, I. S. Elfimov, R. Liang, W. N. Hardy, D. A. Bonn, M. Raudsepp, N. J. C. Ingle, A. Damascelli, $\text{Tl}_2\text{Ba}_2\text{CuO}_{6+\delta}$ brings spectroscopic probes deep into the overdoped regime of the high-Tc cuprates. *New J. Phys.* **9**, 28 (2007).

Acknowledgments: We are grateful to A. V. Chubukov, T. P. Devereaux, S. A. Kivelson, and C. M. Varma for useful discussions. **Funding:** Work at KIT was supported by the Deutsche Forschungsgemeinschaft (DFG, German Research Foundation)—TRR 288-422213477 Elasto-Q-Mat (project A07). R.M.F. was supported by the Air Force Office of Scientific Research under award no. FA9550-21-1-0423. R.M.F. also acknowledges a Mercator Fellowship from the German Research Foundation (DFG) through TRR 288, 422213477 Elasto-Q-Mat. J.S. and R.M.F. acknowledge the hospitality of KITP, where part of this work was done. KITP is supported in part by the National Science Foundation under grant no. NSF PHY-1748958 and NSF PHY-2309135. **Author contributions:** J.S. and R.M.F. conceived and supervised the project.

G.P. and R.O. performed the theoretical analyses. All authors contributed to the paper writing.
Competing interests: The authors declare that they have no competing interests. **Data and materials availability:** All data needed to evaluate the conclusions in the paper are present in the paper.

Submitted 7 December 2023
Accepted 10 May 2024
Published 14 June 2024
10.1126/sciadv.adn3662